Science Advances
AAAS

advances.sciencemag.org/cgi/content/full/5/1/eaau0637/DC1

Supplementary Materials for

A single-stranded coordination copolymer affords heterostructure observation and photoluminescence intensification

Ryojun Toyoda, Ryota Sakamoto*, Naoya Fukui, Ryota Matsuoka, Mizuho Tsuchiya, Hiroshi Nishihara

*Corresponding author. Email: sakamoto@chem.s.u-tokyo.ac.jp.

Published 4 January 2019, *Sci. Adv.* **5**, eaau0637 (2019)
DOI: 10.1126/sciadv.aau0637

This PDF file includes:

Supplementary Materials

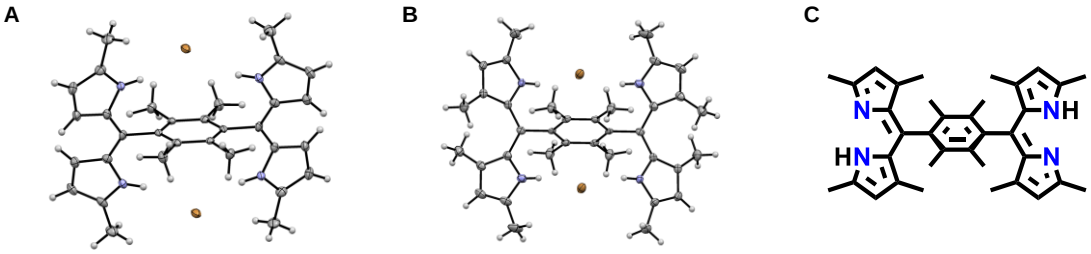

Fig. S1. Oak Ridge thermal ellipsoid plot drawings of H_2L3·2HBr and H_2L3′·2HBr·(solvent)$_n$ with a thermal ellipsoid set at the 50% probability level. Gray: carbon; white: hydrogen; blue: nitrogen; orange: bromine. (**C**) Molecular structure of **H_2L3'**.

Table S1. Crystallographic data.
(A) $H_2L3 \cdot 2HBr$

Empirical Formula	$C_{32}H_{36}Br_2N_4$
Formula Weight / g mol^{-1}	636.47
Temperature / K	93
λ / Å	0.71075
Crystal System	triclinic
Space Group	P-1
a / Å	7.793(3)
b / Å	9.875(4)
c / Å	19.350(8)
α / º	86.845(11)
β / º	87.523(13)
γ / º	78.9714(10)
V / Å^3	1458.6(10)
Z	2
d_{calcd} / g cm^{-3}	1.449
μ (MoKα) / mm^{-1}	2.815
F (000)	652.00
Crystal size / mm^3	0.300×0.300×0.300
Theta range for data collection	3.10 to 27.50 °
Index ranges	-8<=h<=9, -11<=k<=11, -22<=l<=21
Reflections collected	9001
Independent reflections	4619 (R_{int} = 0.0368)
Data completeness	98.2 %
Max. and min. transmission	0.340 and 0.430
Refinement method	Full-matrix least-squares on F^2
Data / restraints / parameters	4619/ 0 / 343
[a] Goodness-of-Fit on F^2	1.096
[b] R_1 [$I > 2.00\sigma(I)$]	0.0431
[c] wR_2 (all reflections)	0.1005
Largest diff. peak and hole / eÅ^{-3}	0.53 and -0.43

(B) $H_2L3'\cdot 2HBr\cdot(Solvent)_n$

Empirical Formula	$C_{36}H_{44}Br_2N_4$
Formula Weight / g mol^{-1}	692.58
Temperature / K	93
λ / Å	0.71073
Crystal System	monoclinic
Space Group	$P2_1/n$
a / Å	9.9254(4)
b / Å	12.8066(5)
c / Å	14.3031(7)
α / ^{o}	90.0000
β / ^{o}	105.514(5)
γ / ^{o}	90.0000
V / Å^3	1751.83(14)
Z	4
d_{calcd} / g cm^{-3}	2.626
μ (MoKα) / mm^{-1}	4.699
F (000)	1432.00
Crystal size / mm^3	0.300×0.300×0.300
Theta range for data collection	2.95 to 31.28 °
Index ranges	-12<=h<=12, -14<=k<=16, -18<=l<=18
Reflections collected	13928
Independent reflections	4014 (R_{int} = 0.0439)
Data completeness	99.9 %
Max. and min. transmission	0.782 and 1.000
Refinement method	Full-matrix least-squares on F^2
Data / restraints / parameters	4014/ 0 / 190
[a] Goodness-of-Fit on F^2	1.042
[b] R_1 [$I > 2.00\sigma(I)$]	0.0394
[c] wR_2 (all reflections)	0.0908
Largest diff. peak and hole / eÅ^{-3}	0.41 and -0.36

The contribution of solvent electron density was removed by the SQUEEZE function.

[a]GOF = $[\Sigma(w(Fo^2 - Fc^2)^2/\Sigma(Nr - Np)^2]$. [b] $R_1 = \Sigma||Fo| - |Fc||/\Sigma|Fo|$ ($I > 2\ \sigma\ (I)$).

[c]$wR_2 = [\Sigma(w(Fo^2 - Fc^2)^2/\Sigma w(Fo^2)^2]^{1/2}$ ($I > 2\ \sigma(I)$).

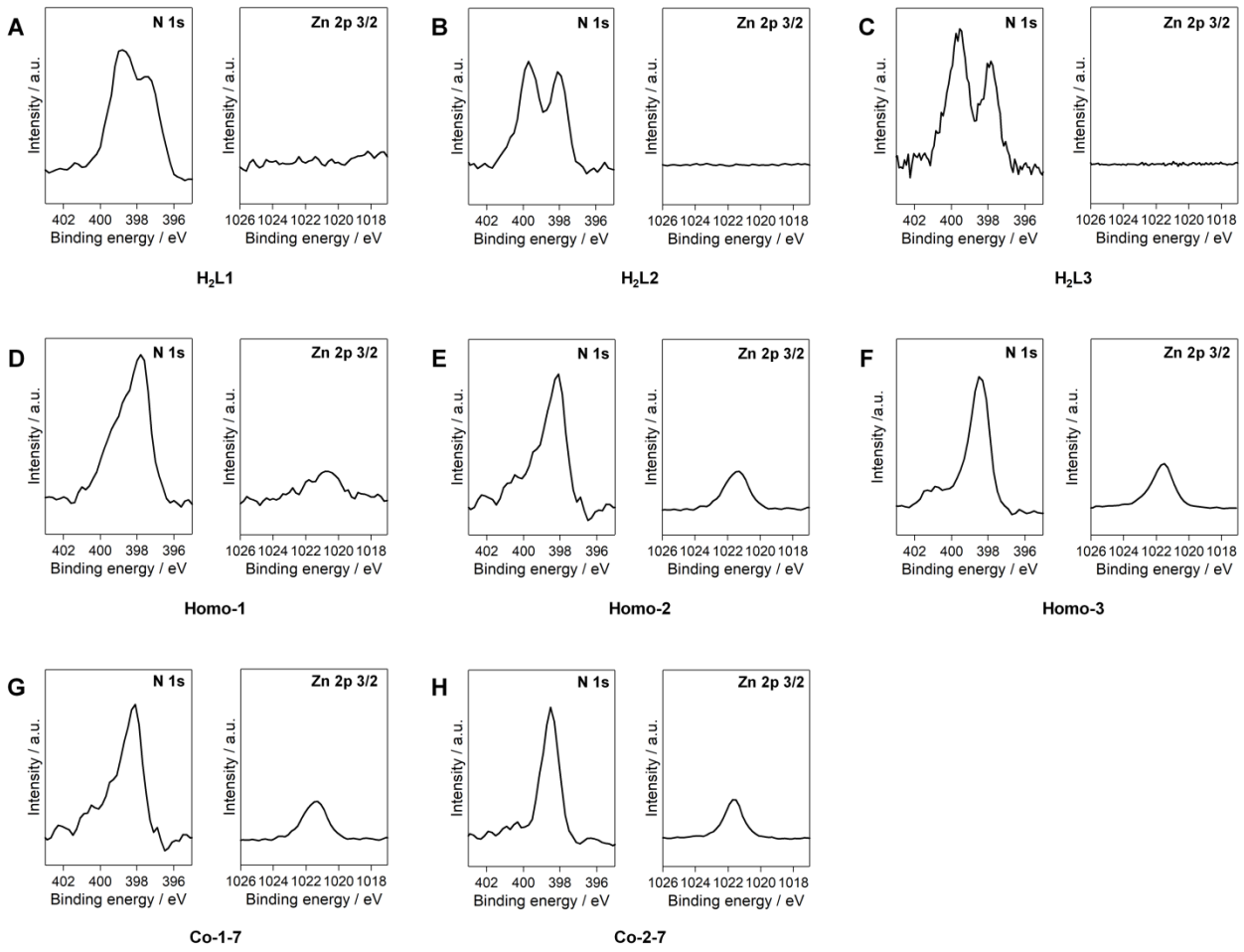

Fig. S2. XPS for proligands and coordination polymers. (**A**) **H_2L1**. (**B**) **H_2L2**. (**C**) **H_2L3**. (**D**) **Homo-1**. (**E**) **Homo-2**. (**F**) **Homo-3**. (**G**) **Co-1-*7***. (**H**) **Co-2-*7***. The intensity of the signal is standardized using the photoionization cross-section of each element.

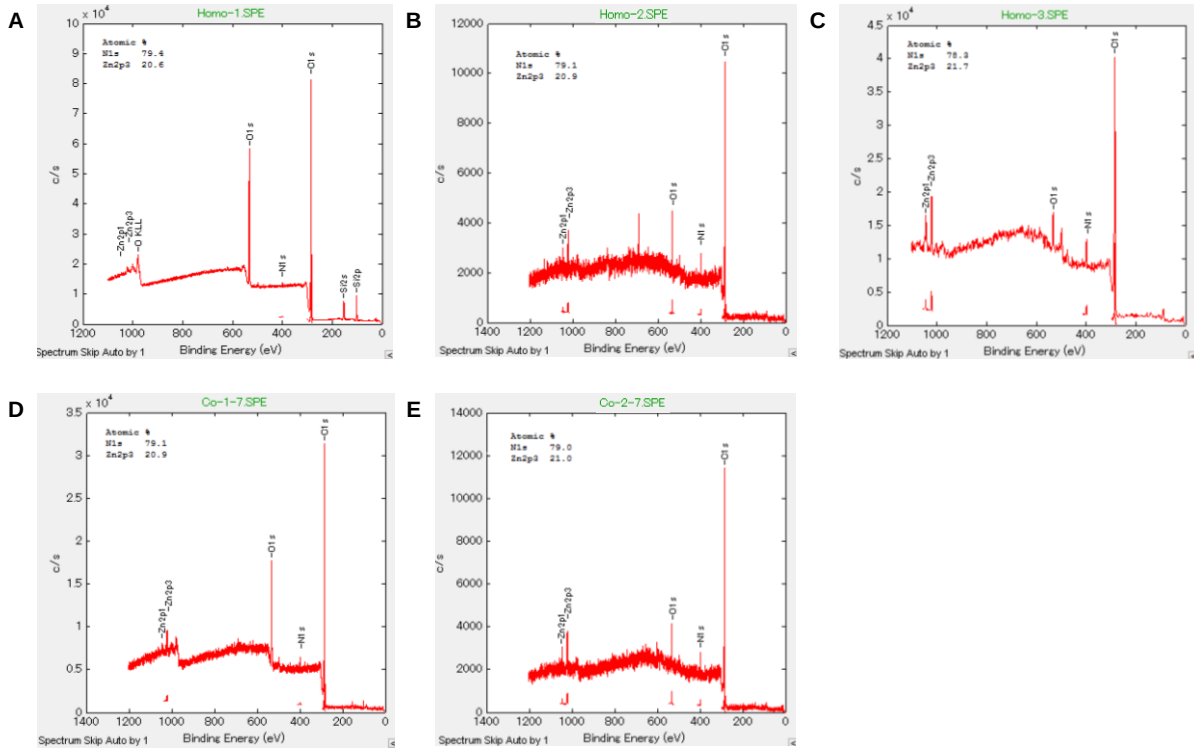

Fig. S3. Quantification of the elemental ratio from XPS. (**A**) **Homo-1**. (**B**) **Homo-2**. (**C**) **Homo-3**. (**D**) **Co-1-*7***. (**E**) **Co-2-*7***.

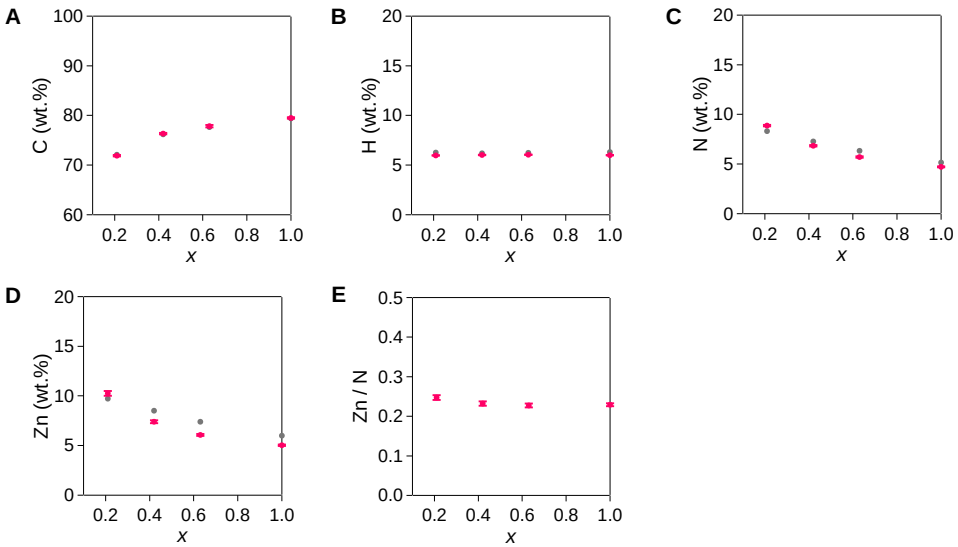

Fig. S4. Elemental abundances in Co-1-*k* and Homo-1 determined by elemental and ICP-AES analysis. (**A**) carbon; (**B**) hydrogen; (**C**) nitrogen; (**D**) zinc. (**E**) Zn/N-***x*** plot. As an admixture, water molecules were added; 2.12, 1.53, 0.87 and 1.31 molecules per zinc center were added to **Homo-1**, **Co-1-*k*** with ***x*** = 0.21, 0.42, and 0.63, respectively. Gray: calculated; magenta: experimental.

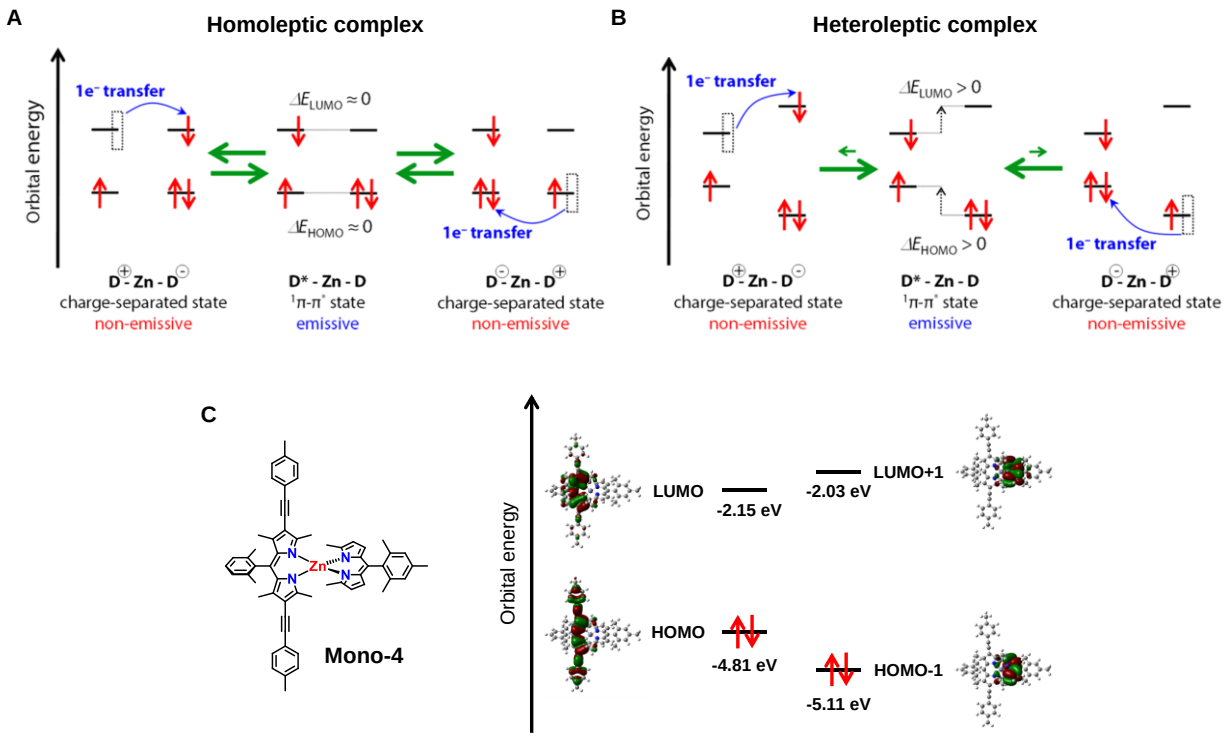

Fig. S5. PL enhancement mechanism for a heteroleptic complex. (**A**,**B**) Schematic illustrations of plausible thermal equilibria among the two non-emissive symmetry-breaking charge-separated states and the emissive $^{1}\pi$–π^{*} excited state localized on the left-hand dipyrrinato ligand in the case of (**A**) homoleptic complex; (**B**) heteroleptic complex. (**C**) Chemical structure and molecular orbitals of **Mono-4** with DFT/B3LYP/6-31G(d).

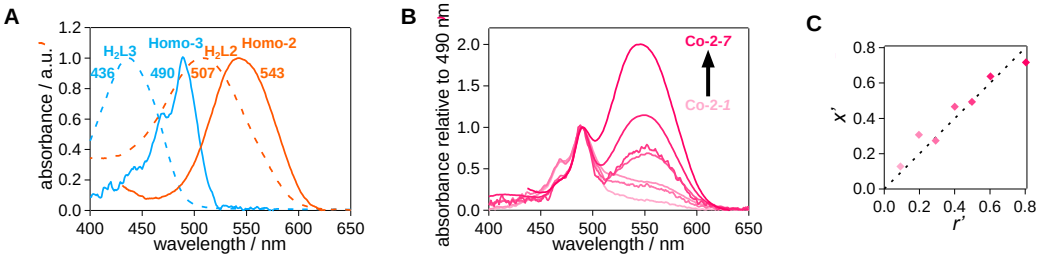

Fig. S6. UV/vis spectroscopy for Co-2-*k* in toluene. (**A**) Normalized UV/vis spectra of bridging dipyrrin proligands **H₂L2** and **H₂L3**, and homopolymers **Homo-2** and **Homo-3**. (**B**) UV/vis spectra of **Co-2-*k*** (*k* = 1–7) normalized at 490 nm. (**C**) Relationship between the mole fraction of **L2** in **Co-2-*k*** (***x'***) and mixing ratio of **H₂L2** to (**H₂L2** + **H₂L3**) (***r'***).

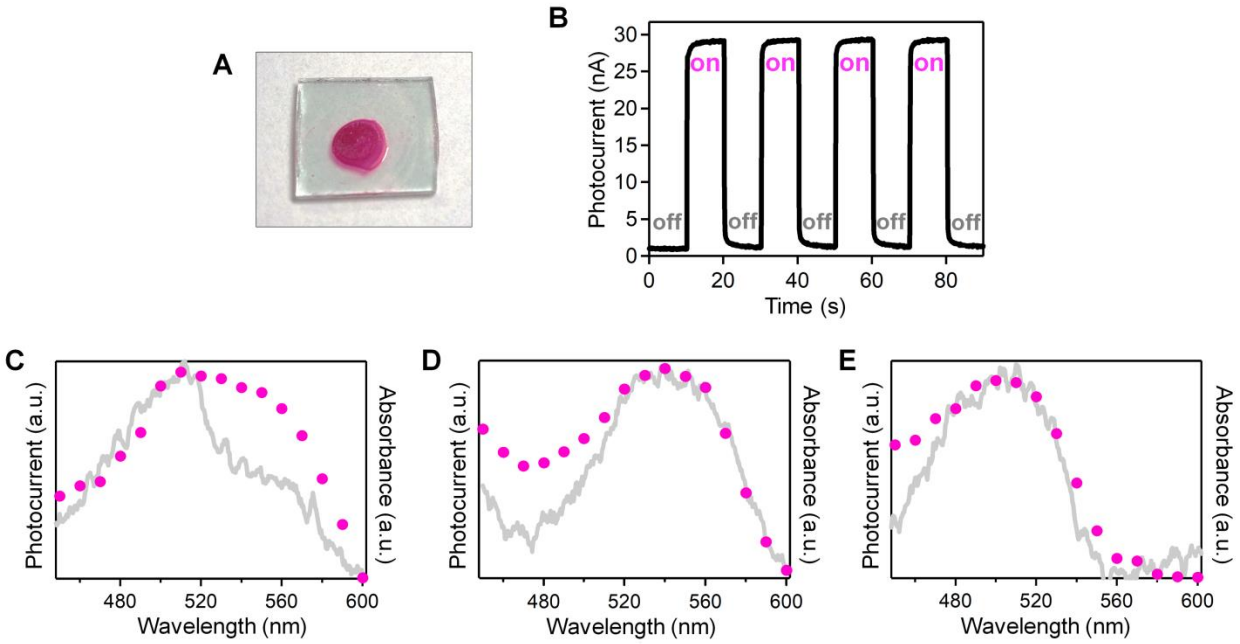

Fig. S7. Photovoltaic conversion of Co-1-6, Homo-3, and Homo-1. (**A**) Photograph of a thin film of **Co-1-*6*** on a SnO_2 substrate. (**B**) Anodic photocurrent response of **Co-1-*6*** on irradiation of an electrode with intermittent 500 nm light (Light intensity: 3.56 mW). (**C**) Action spectrum for the photocurrent generation and absorption spectrum of **Co-1-*6*** on a SnO_2 substrate. (**D**) Action spectrum for the photocurrent generation and absorption spectrum of **Homo-3** on a SnO_2 substrate. (**E**) Action spectrum for the photocurrent generation and absorption spectrum of **Homo-1** on a SnO_2 substrate.

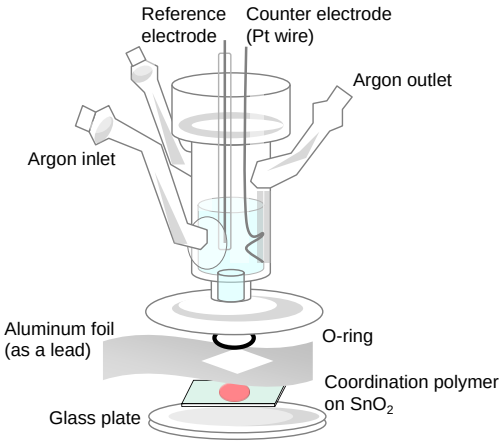

Fig. S8. Three-electrode electrochemical cell used for the photoelectric conversion. The incident light was illuminated from the bottom of the cell.

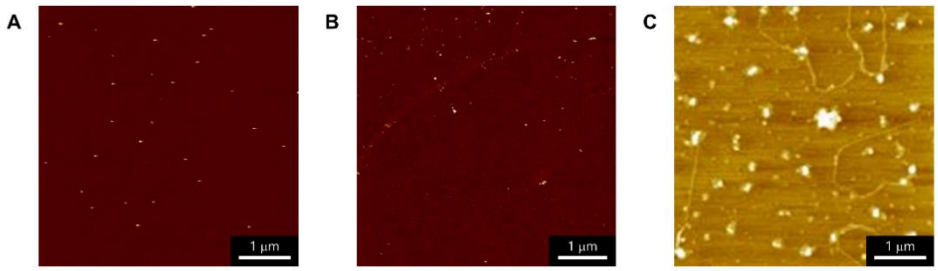

Fig. S9. AFM images of Co-1-3 on other substrates. (**A**) On mica. (**B**) On SiO_2/Si(100). (**C**) On MoS_2. Among those, only MoS_2 visualized the exfoliated **Co-1-*3***.

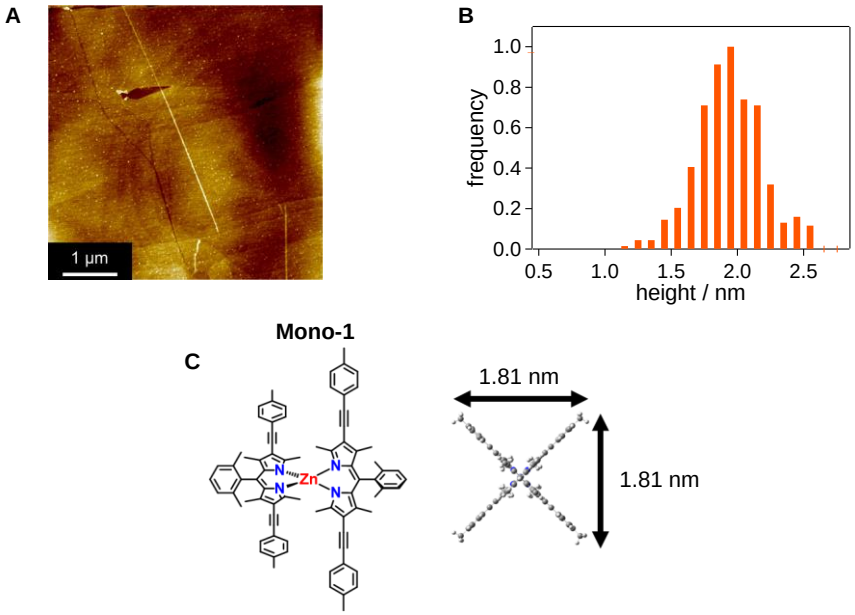

Fig. S10. AFM for Homo-1. (**A**) Representative AFM height image for **Homo-1**. (**B**) Height histogram. (**C**) Chemical structure of corresponding mononuclear complex **Mono-1**, with a size estimated by DFT calculation.

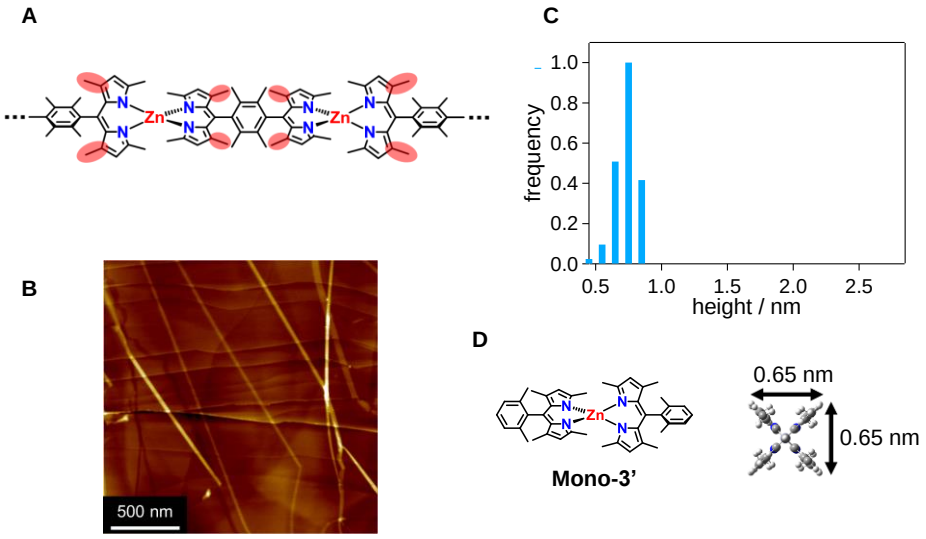

Fig. S11. AFM for Homo-3′. (**A**) Molecular structure of **Homo-3'**. The difference between **Homo-3** lies in additional methyl groups shown in red. The lower dispersibility of **Homo-3** hampered the AFM analysis, which prompted us to use **Homo-3'** as an alternative. The additional methyl group is unlikely to alter the height of the single strand observed in AFM. (**B**) Representative AFM height image for **Homo-3'**. (**C**) Height histogram. (**D**) Chemical structure of corresponding mononuclear complex **Mono-3''**, with a size estimated by DFT calculation.

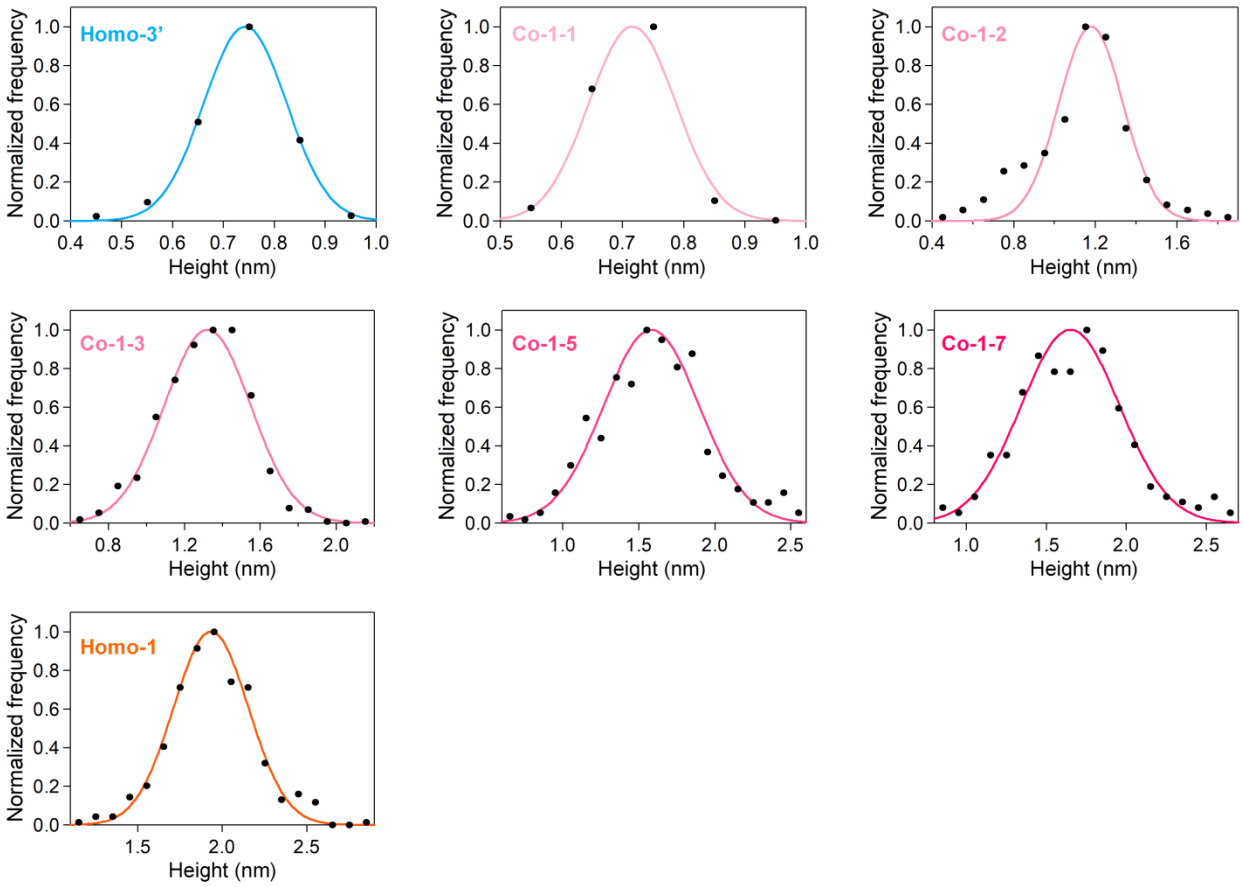

Fig. S12. Gaussian fitting of AFM height histograms of Co-1-*k*, Homo-1, and Homo-3′.

Table S2. PL properties of Co-1-*k*, Homo-1, and Homo-3 in toluene.

Sample	ϕ_{PL} (excited at 550 nm)	ϕ_{PL} (excited at 490 nm)	τ_{PL} /ns
Co-1-*1*	0.32	0.21	2.89 [a]
Co-1-*2*	0.24	0.23	2.72 [a]
Co-1-*3*	0.25	0.25	2.66 [a]
Co-1-*4*	0.15	0.15	2.46 [a]
Co-1-*5*	0.12	0.12	2.16 [a]
Co-1-*6*	0.11	0.11	2.08 [a]
Co-1-*7*	0.06	0.06	1.61 [a]
Homo-1	0.03	N/A	N/A [b]
Homo-3	N/A	0.10	3.79 [a]

[a] measured at excitation with 470 nm. [b] not measured due to low absorption at 470 nm.

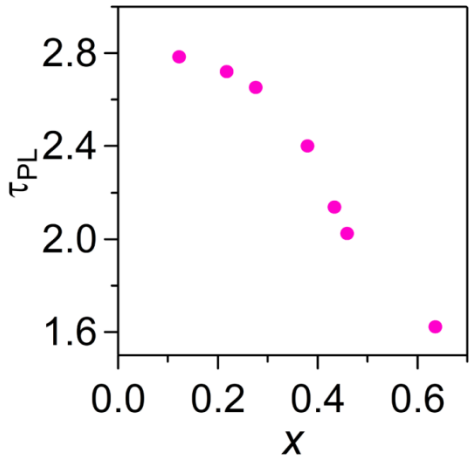

Fig. S13. PL lifetimes (τ_{PL}) in toluene. τ_{PL} – mole ratio of ligand **L1** (***x***) plots. PL lifetime of **Co-1-*k*** was measured in toluene with an incident light of 470 nm. The PL decay was fitted with a single-exponential decay.

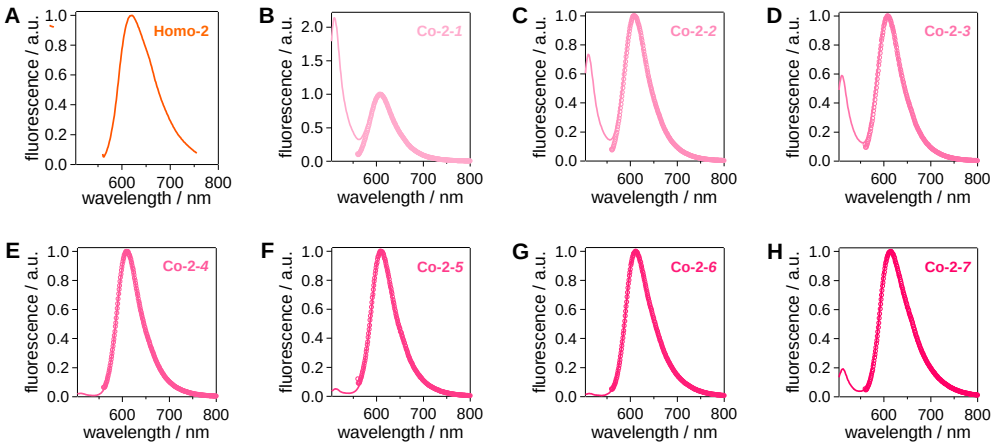

Fig. S14. PL of Co-2-*k* in toluene. PL spectra of (**A**) **Homo-2** excited at 550 nm. (**B**–**H**) **Co-2-*k*** (*k* = 1–7) excited at 490 (solid line) and 550 nm (circle).

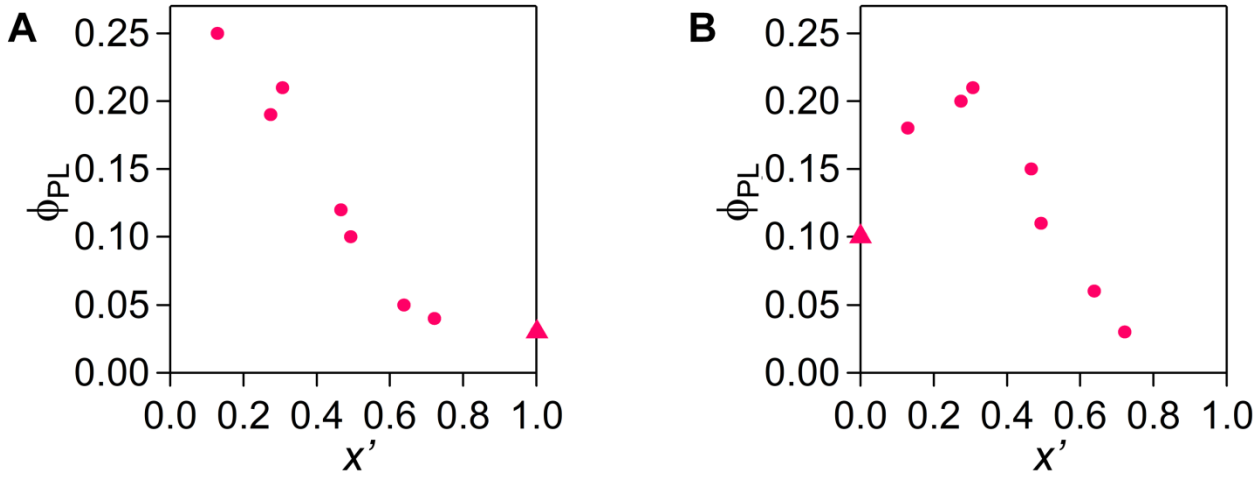

Fig. S15. PL quantum yield dependence on *x′* in toluene. (**A**,**B**) $\phi_{PL} - x'$ plots for coordination copolymers **Co-2-*k*** (*k* = 1–7; circles) and homopolymers **Homo-2** and **Homo-3** (triangles) excited at (**A**) 550 nm; (**B**) 490 nm.

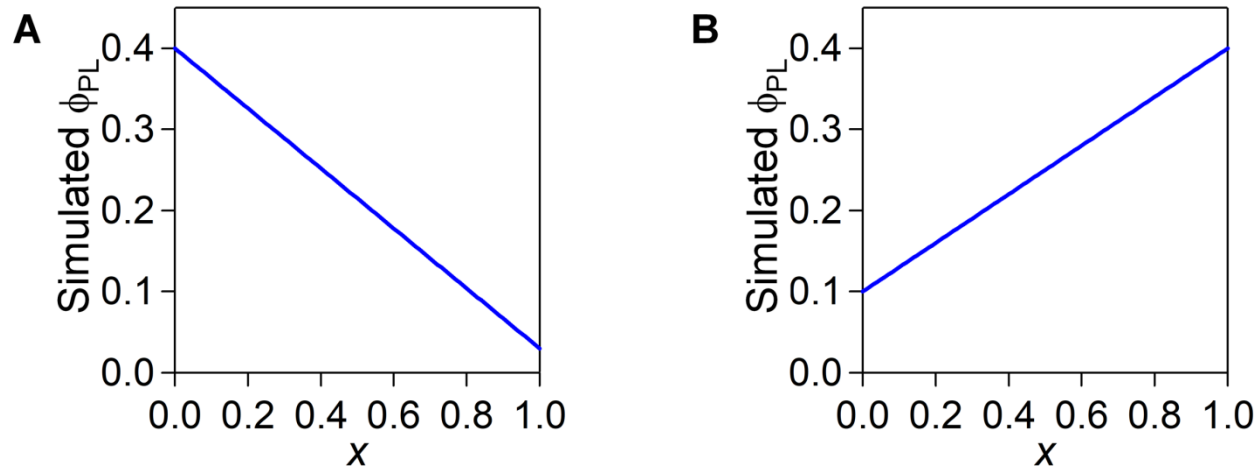

Fig. S16. Calculated ϕ_{PL} dependence on *x*. (**A**) When excited at 550 nm; (**B**) When excited at 490 nm. Herein, intrawire exciton hopping is not considered. For 550 nm illumination, $\mathbf{D_{Homo\text{-}L1}}$ or $\mathbf{D_{Hetero\text{-}L1}}$ is photoexcited, the distribution ratio of which is $x : (1 - x)$. Therefore, the simulated $\phi_{PL} = \phi(\mathbf{D_{Homo\text{-}L1}})\, x + \phi(\mathbf{D_{Hetero\text{-}L1}})\,(1 - x)$, where $\phi(\mathbf{D_{Homo\text{-}L1}})$ and $\phi(\mathbf{D_{Hetero\text{-}L1}})$ denote the probabilities of PL emission from $\mathbf{D_{Homo\text{-}L1}}$ and $\mathbf{D_{Hetero\text{-}L1}}$. For 490 nm illumination, $\mathbf{D_{Homo\text{-}L3}}$ or $\mathbf{D_{Hetero\text{-}L3}}$ is photoexcited, the distribution ratio of which is $(1 - x) : x$. Therefore, the simulated $\phi_{PL} = \phi(\mathbf{D_{Homo\text{-}L3}})\,(1 - x) + \phi(\mathbf{D_{Hetero\text{-}L3}})\, x$, where $\phi(\mathbf{D_{Homo\text{-}L3}})$ and $\phi(\mathbf{D_{Hetero\text{-}L3}})$ denote the probabilities of PL emission from $\mathbf{D_{Homo\text{-}L3}}$ and $\mathbf{D_{Hetero\text{-}L3}}$. $\phi(\mathbf{D_{Homo\text{-}L3}}) = 0.10$; $\phi(\mathbf{D_{Homo\text{-}L1}}) = 0.03$; $\phi(\mathbf{D_{Hetero\text{-}L3}}) = \phi(\mathbf{D_{Hetero\text{-}L1}}) = 0.40$, the same value used in the numerical simulation shown in Fig. 6C.

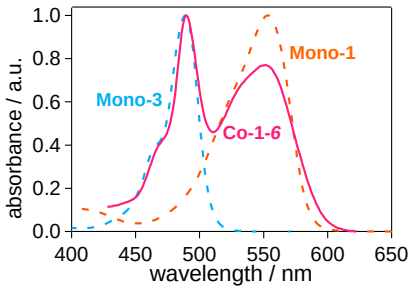

Fig. S17. UV/vis absorption spectroscopy for copolymers and corresponding mononuclear complexes in toluene. UV/vis spectra of **Co-1-*6*** (solid line), **Mono-1** (dotted line, orange) and **Mono-3** (dotted, blue).